Heat Transfer Engineering

ISSN: 0145-7632 (Print) 1521-0537 (Online) Journal homepage: http://www.tandfonline.com/loi/uhte20

Large Eddy Simulation of Normally Impinging Round Air-Jet Heat Transfer at Moderate Reynolds Numbers

Yongping Li, Liang Zhang, Qizhao Lin & Zuojin Zhu

To cite this article: Yongping Li, Liang Zhang, Qizhao Lin & Zuojin Zhu (2017) Large Eddy Simulation of Normally Impinging Round Air-Jet Heat Transfer at Moderate Reynolds Numbers, Heat Transfer Engineering, 38:17, 1439-1448, DOI: 10.1080/01457632.2016.1255077

To link to this article: http://dx.doi.org/10.1080/01457632.2016.1255077

Accepted author version posted online: 03 Nov 2016.
Published online: 03 Nov 2016.

Submit your article to this journal

Article views: 21

View related articles

View Crossmark data

Full Terms & Conditions of access and use can be found at
http://www.tandfonline.com/action/journalInformation?journalCode=uhte20

Download by: [University of Science and Technology of China] **Date:** 21 April 2017, At: 16:49

HEAT TRANSFER ENGINEERING
2017, VOL. 38, NO. 17, 1439–1448
http://dx.doi.org/10.1080/01457632.2016.1255077

Taylor & Francis
Taylor & Francis Group

Large Eddy Simulation of Normally Impinging Round Air-Jet Heat Transfer at Moderate Reynolds Numbers

Yongping Li[a], Liang Zhang[b], Qizhao Lin[a], and Zuojin Zhu[c]

[a]Department of Thermal Science and Energy Engineering, USTC, Hefei, China; [b]Research Institute of Chemical Defense, The 5th Department, Beijing, China; [c]Faculty of Engineering Science, USTC, Hefei, China

ABSTRACT
This paper presents results of dynamic Smagorinsky-type model-based large eddy simulation of normally impinging round air-jet heat transfer at moderate Reynolds numbers (4,400, 10^4, and 2.3×10^4) with orifice-to-plate distance fixed at 5. Using software Open Source Field Operation and Manipulation (OpenFOAM), predicted distributions of mean velocity components, velocity fluctuations, and turbulent stresses in the vertical and radial directions are compared with existing empirical and numerical results. For the predicted heat flow from the target wall, there is satisfactory consistency of the mean Nusselt number in comparison with measured empirical results.

1. Introduction

To enhance heat transfer, jet impingement is a conventional method [1,2]. Increasing the normal velocity gradient and turbulence intensity of fluid flow near the impingement surface, can improve the heat transfer [3]. As ice on highways and urban roads in winter are harmful, with significant influence on the safety of car-drivers and travelers, it generates a demand of effective ice-removal tool. Furthermore, the study of impinging round jet heat transfer has great significance in thermal science. Before introducing the main objective of this paper, background of impinging jet heat transfer, categorized into the experimental [3–14] and numerical aspect [15–28] is briefly reported below.

Many numerical studies have been completed by means of direct numerical simulation (DNS), Reynolds averaged Navier–Stokes (RANS) modeling, and large eddy simulation (LES). In RANS simulation, Craft et al. [15] employed an extended version of the finite-volume code TEAM to predict turbulent impinging jets discharged from a circular pipe, measured by Baughn and Shimizu [5] and Cooper et al. [6]. Zhang et al. [18] studied flow and heat transfer performance of a deflector under periodic jet impingement with the k-ε model developed by using Re-Normalization Group (RNG) methods [19].

LES of a forced semi-confined round impinging jet were done by Olsson and Fuchs [20]. For the case of Reynolds number of 10^4, the inflow was forced at a Strouhal number of 0.27, the orifice-to-plate distance was set at $H/D = 4$. The existence of separation vortices in the wall jet region was confirmed, and secondary vortices were found to be related to the radially deflected primary vortices generated by the circular shear layer of the jet, while primary vortex structures that reach the wall were helical and not axi-symmetric.

LES results of round impinging air jets with heat transfer were reported by Hällqvist [21]. In particular, the LES model was a basic one without explicit sub-grid-scale (SGS) modeling and without explicit filtering. Instead, the numerical scheme was used to consider the necessary amount of dissipation. It was found that top-hat and turbulent inflow conditions can yield a higher rate of incoherent small-scale structures. The applied *swirl* level at the velocity inlet has significant influence on the rate of heat transfer. The turbulence level increased with swirl, which was positive for heat transfer, and also the jet spreading.

Based on LES of a normally impinging round jet issuing from a long pipe at a Reynolds number Re $= 2 \times 10^4$, and $H/D = 2$, Hadžiabdic and Hanjalic [22] found that there were interesting time and spatial dynamics of the vorticity and eddy structures and their imprints on target wall. Uddin et al. [23] performed LES of turbulent jets that normally impinge on a target surface, focused on the case of a jet that was issued from a circular pipe into stagnant

CONTACT Professor Zuojin Zhu zuojin@ustc.edu.cn Faculty of Engineering Science, University of Science and Technology of China (USTC), Hefei 230026, China.
Color versions of one or more of the figures in this paper can be found online at www.tandfonline.com/uhte.
© 2017 Taylor & Francis Group, LLC

surrounding air at the relatively high jet-issuing Reynolds number of 2.3×10^4 and $H/D = 6$. They found that only one of the models considered succeeded in representing effects on the heat fluxes of the complex strain field associated with the stagnation region and the subsequent development into the wall jet region, and discussed the relevant reasons.

More recently, based on the singular valued SGS model [24] with LES results compared with those based on the dynamic Smagorinsky model [25], recent development of computation of turbulent impinging jet heat transfer was reported by Dewan et al. [26]. An LES-dedicated prediction of a pulsatile hot-jet impinging a flat-plate in the presence of a cold turbulent cross-flow was conducted by Toda et al. [27], in which two eddy-viscosity-based SGS models, i.e., the σ-model [24] and the dynamic Smagorinsky model [25] were used. LES of a turbulent jet impinging on a heated wall using high-order numerical schemes were carried out by Dairay et al. [28], indicating that highly accurate numerical methods could lead to correct predictions of velocity statistics and heat transfer but only if a procedure was used to regularize the large-scale dynamics calculated explicitly.

The brief literature review reported above shows that the impinging jet heat transfer is certainly a hot topic in research. Considering the mechanism of impinging jet heat transfer being helpful to the design of effective ice-removal tool, and the case at shorter orifice-to-plate distance ($H/D = 2$) has been numerically investigated [22,28], we focus in this study on investigating the normally impinging round air-jet heat transfer at a relatively long orifice-to-plate distance ($H/D = 5$) at moderate jet-issuing Reynolds numbers (4,400, 10^4, and 2.3×10^4) by LES on the basis of the dynamic Smagorinsky model [25] using calculation based on the open source-code OpenFOAM (Open Source Field Operation and Manipulation). The distributions of mean velocities, their fluctuations, mean Nusselt numbers, and the corresponding dependence of air-jet Reynolds number are discussed in the section of results and discussion.

2. Governing equations

Schematically, the jet heat transfer problem is shown in Figure 1. It involves a round air-jet impinging normally to a plat plate, with a fixed relatively long orifice-to-plate distance of $H/D = 5$. The jet Reynolds numbers ($\mathrm{Re} = W_b D/\nu$) for the LES are, respectively, 4,400, 10^4, and 2.3×10^4, at which the flows are turbulent [23]. For simplicity, air temperature of the jet is assumed to be the same as the ambient temperature, but lower than that of the plate surface heated under the condition of constant heat flux. The air jet plays a cooling role on the target wall. Although

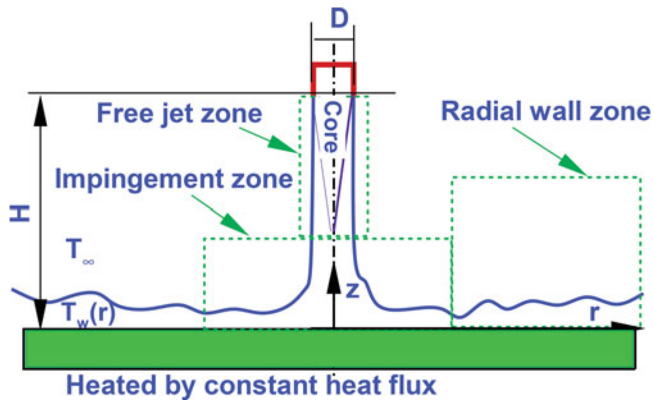

Figure 1. Schematic diagram of normally impinging round air-jet heat transfer.

there exists a reverse effect in the case of ice-removal, the mechanism of jet impinging heat transfer is almost the same as soon as the ice melting related phenomenon is excluded. It is assumed that the air jet flow is incompressible, the cooling mode is mainly related to forced convection, the contributions due to buoyancy caused natural convection, and wall thermal radiation are negligible. Following the published work [17,23], using these assumptions and the mass, momentum and energy conservations, the governing equations can be written as

$$\frac{\partial \widehat{u}_i}{\partial x_i} = 0 \tag{1}$$

$$\frac{\partial \widehat{u}_i}{\partial t} + \frac{\partial (\widehat{u}_j \widehat{u}_i)}{\partial x_j} = -\frac{1}{\rho}\frac{\partial \widehat{p}}{\partial x_i} + \nu \frac{\partial}{\partial x_j}\left[\frac{\partial \widehat{u}_i}{\partial x_j} + \frac{\partial \widehat{u}_j}{\partial x_i}\right] - \frac{1}{\rho}\frac{\partial \tau_{ij}^s}{\partial x_j} \tag{2}$$

$$\frac{\partial (c_p \widehat{T})}{\partial t} + \frac{\partial (c_p \widehat{u}_j \widehat{T})}{\partial x_j} = \frac{1}{\rho}\frac{\partial}{\partial x_j}\left[\Gamma c_p \frac{\partial \widehat{T}}{\partial x_j}\right] - \frac{1}{\rho}\frac{\partial q_j^s}{\partial x_j} \tag{3}$$

where ν, ρ, c_p, and Γ are thermophysical parameters of air, u_i is the flow velocity component in the x_i direction, T represents air temperature, with the over hat $'\widehat{\ }'$ denoting the resolved variables. Sub-grid scale stress is defined by

$$\tau_{ij}^s = \rho(\widehat{u_i u_j} - \widehat{u}_i \widehat{u}_j). \tag{4}$$

The sub-grid scale closure model for momentum is based on a gradient-diffusion hypothesis, which can be expressed as a relation between anisotropic stress and (large-scale) strain rate tensor:

$$\tau_{ij}^s - \frac{1}{3}\delta_{ij}\tau_{kk}^s = 2\rho\nu_s\left(\widehat{S}_{ij} - \frac{1}{3}\delta_{ij}\widehat{S}_{kk}\right), \tag{5}$$

where ν_s is sub-grid viscosity, given by

$$\nu_s = (c_s\Delta)^2\widehat{S} = (c_s\Delta)^2\sqrt{2\widehat{S}_{ij}\widehat{S}_{ij}}, \tag{6}$$

Table 1. Thermophysical properties of air used in the LES.

$\rho(\mathrm{kg/m^3})$	$c_p(\mathrm{kJ/kg\cdot K})$	$\lambda(\mathrm{W/m\cdot K})$	$\nu(\mathrm{m^2/s})$	Pr
1.1767	1.0066	0.0262	1.58×10^{-5}	0.7196

where

$$\widehat{S}_{ij}=\frac{1}{2}\left(\frac{\partial\widehat{u}_i}{\partial x_j}+\frac{\partial\widehat{u}_j}{\partial x_i}\right) \tag{7}$$

is the resolved strain rate. In Eq. (6), Δ is the grid filter width, c_s is a constant determined by Germano identity dynamically, which assumes similarity of SGS quantities between the *grid* (Δ) filter level and the *test* $(\sim 2\Delta)$ filter level [29], implying that the sub-grid scale model employed is the dynamic Smagorinsky-type model (DSM) [30].

Sub-grid heat flux q_j^s is expressed as

$$q_j^s=\rho c_p(\widehat{u_jT}-\widehat{u}_j\widehat{T}). \tag{8}$$

Again, let Pr_s be sub-grid Prandtl number, and using gradient diffusion assumption as reported in Ref. [23], we have

$$q_j^s=-\rho c_p\alpha_s\frac{\partial\widehat{T}}{\partial x_j}, \tag{9}$$

where $(\alpha_s=\nu_s/\mathrm{Pr}_s)$ denotes sub-grid thermal diffusivity. In the present LES, the sub-grid Prandtl number Pr_s is set at 0.85.

The open boundaries at the top and side are assigned to have constant pressure conditions, which allow the occurrence of possible reverse flow. The inflow turbulence intensity is assumed at the level of 1%, so that the root mean square (rms) value of velocity fluctuation for each component can be simply set as 1% of the jet velocity W_b. On the target plate wall, no-slip condition and constant heat flux condition are used. The heat flux was set at 1,000 $\mathrm{W/m^2}$, similar to that described in Ref. [23]. While the ambient air temperature in this LES is set at 300K, at which the thermo-physical properties under standard atmospheric pressure are given in Table 1.

It is noted that the artificially assumed heat flux almost certainly has no impact on the calculated value of Nusselt number, since heat transfer mechanism is primarily dominated by turbulent forced convection caused by the air-jet impinging.

3. Numerical method

LES is carried out by virtue of control volume approach in an unstructured grid system. For the discretization of governing Eqs. (1)–(3), second-order Crank–Nicolsen method is used for time derivatives, while the second-order central-difference scheme is used for spatial partial derivatives. The discretized algebraic equations are solved by the PISO (Pressure Implicit with Splitting of Operator) algorithm.

Table 2. Computational parameters.

Re	$W_b(\mathrm{m/s})$	z^+	$t_0(\mathrm{s})$	$\overline{\tau}$	R_s
4,400	9.96	≤ 1.87	7.049×10^{-3}	5806	32.26
10,000	22.57	≤ 1.96	3.101×10^{-3}	3398	125.3
23,000	51.91	≤ 3.59	1.348×10^{-3}	2789	351.1

Note that time step (Δt) in OpenFOAM is self-adjusted. It is achieved by assigning a condition that the Courant number be less than 0.5, i.e., $\Delta t|U|/\delta x<0.5$, where δx refers to the cell size in the direction of velocity, and $|U|$ refers to the magnitude of velocity through that cell. The total cell number is about 1.2×10^6. As shown in the third column of Table 2, the normalized finest grid distance close to the target wall ($z^+=zu_\tau/\nu$, u_τ refers to the friction velocity) is less than 1.87, 1.96, or 3.59 for jet Reynolds number ($\mathrm{Re}=W_bD/\nu$) of 4,400, 10^4, or 2.3×10^4, respectively, causing the time step sometimes at the level of micro-second. For heat transfer problems in engineering, $z^+\leq 5$ may be a relatively suitable choice [31]. Grid distribution near the stagnation point can be seen in Figure 2.

LES calculation is encompassed using a single processor of a parallel computer station. Computational parameters are listed in Table 2, where the sixth column shows the step ratio R_s estimated on the approach reported by Smirnov et al. [32]. The so-called step ratio refers to the ratio of maximal allowable number of time steps for the problem and the actual number of time steps used to obtain the result. For $S^{\max}\approx 3\%$, R_s values are all larger than 30, as shown in Table 2.

For estimating the accumulated error in numerical work based on Navier–Stokes equations, the step ratio R_s can be used. As reported by Smirnov et al. [32], R_s characterizes reliability of results to determine the limit of the simulations. The higher the value of R_s, the lower the accumulated error is. As R_s approaches unity, the error tends to a maximum allowable value. As the reliability of numerical results is evaluated by a step ratio approach [32], the relevant verification is done in comparison with measured empirical correlation, thus omitting the checking of grid independence. The DSM-based LES results will be discussed in the next section.

4. Results and discussion

Taking, respectively, the jet-nozzle diameter D and the jet speed W_b as the scales of length and velocity, the time scale t_0 is D/W_b. As the jet nozzle diameter D is chosen as 0.007 m in this LES, relevant values of the time scale (t_0), jet

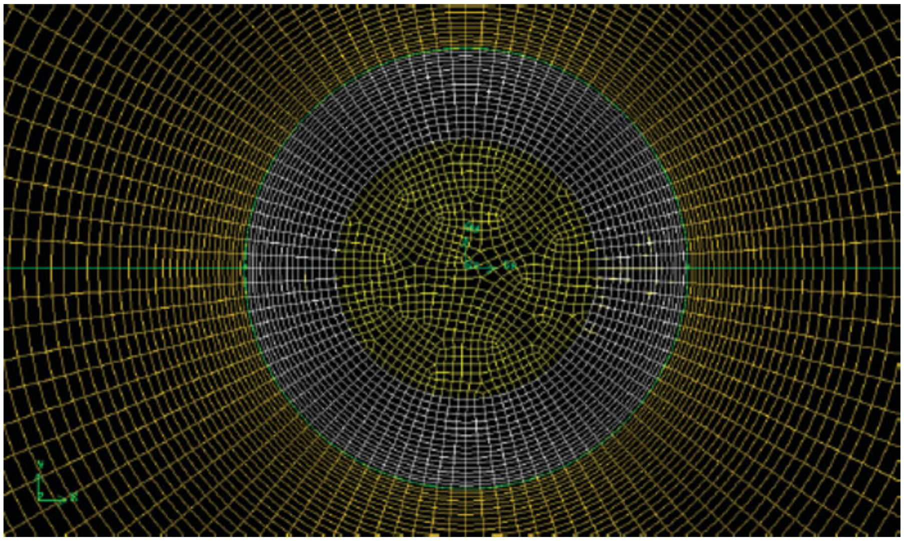

Figure 2. Grid distribution near the stagnation point in the x–y plane.

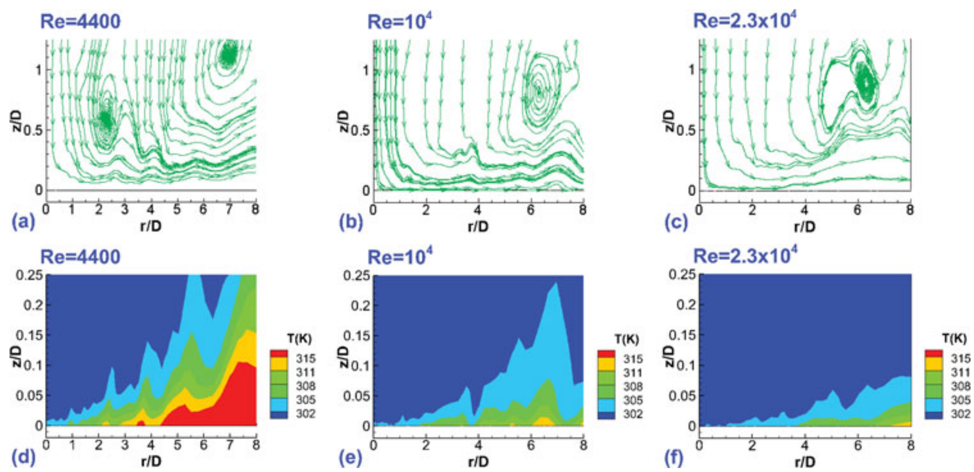

Figure 3. Instantaneous streamlines and temperature contours in the near wall region (a) $\bar{t} = 5801.96$, Re$=$ 4,400; (b) $\bar{t} = 278.8$, Re $= 10^4$; (c) $\bar{t} = 302.4$, Re $= 2.3 \times 10^4$.

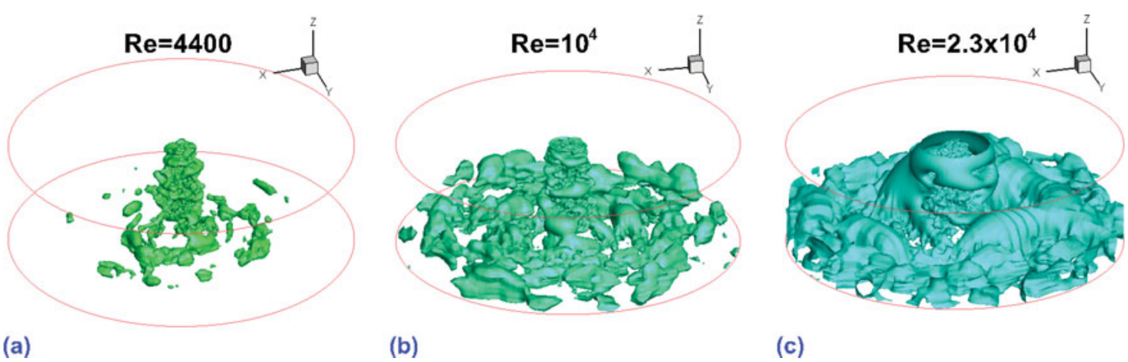

Figure 4. Instantaneous iso-surface of pressure fluctuation at different Reynolds numbers, (a) $\bar{t} = 5801.96$, Re $=$ 4,400; (b) $\bar{t} = 278.8$, Re $= 10^4$; (c) $\bar{t} = 302.4$, Re $= 2.3 \times 10^4$. Note that the iso-surface of pressure fluctuation is labeled by -1.18Pa.

velocity (W_b), and time period for the statistical analysis ($\overline{\tau}$) are shown in Table 2.

To show the flow structures of impinging jet on the target plate, instantaneous streamlines for the three cases are shown in Figures 3 a–c, with the illustrations of temperature contours shown in Figures 3 d–f. It can be seen that the locations of the deflected primary vortices and their shapes not only vary temporally and spatially under the turbulent flow regime, but also depend on the jet Reynolds number (Re).

As the target wall is heated under constant heat flux, air temperature in the wall region has an intimate dependency on Re, with an increase of Re, for a given point in the $r - z$ plane, it has a lower value. The temperature patterns in Figures 3 d–f indicate the heat transfer rate due to air-jet impingement is intimately dependent on Re.

To further illustrate the jet Re dependence, Figures 4a–c give instantaneous iso-surface of pressure fluctuations labeled by the value -1.18Pa. This pressure iso-surface indicates that the impinging jet flow does relate to the intensity of fluid–solid interaction, which depends on the jet momentum flux and orifice-to-plate distance.

Figures 5 a–c show maps of normalized mean velocity magnitude and mean turbulent kinetic energy. Although these maps of mean velocity magnitude are almost insensitive to the jet Re, the maps of the mean turbulent kinetic energy $\langle k\rangle/W_b^2$ reveal that mean contours of $\langle k\rangle/W_b^2$ are slightly sensitive to Re.

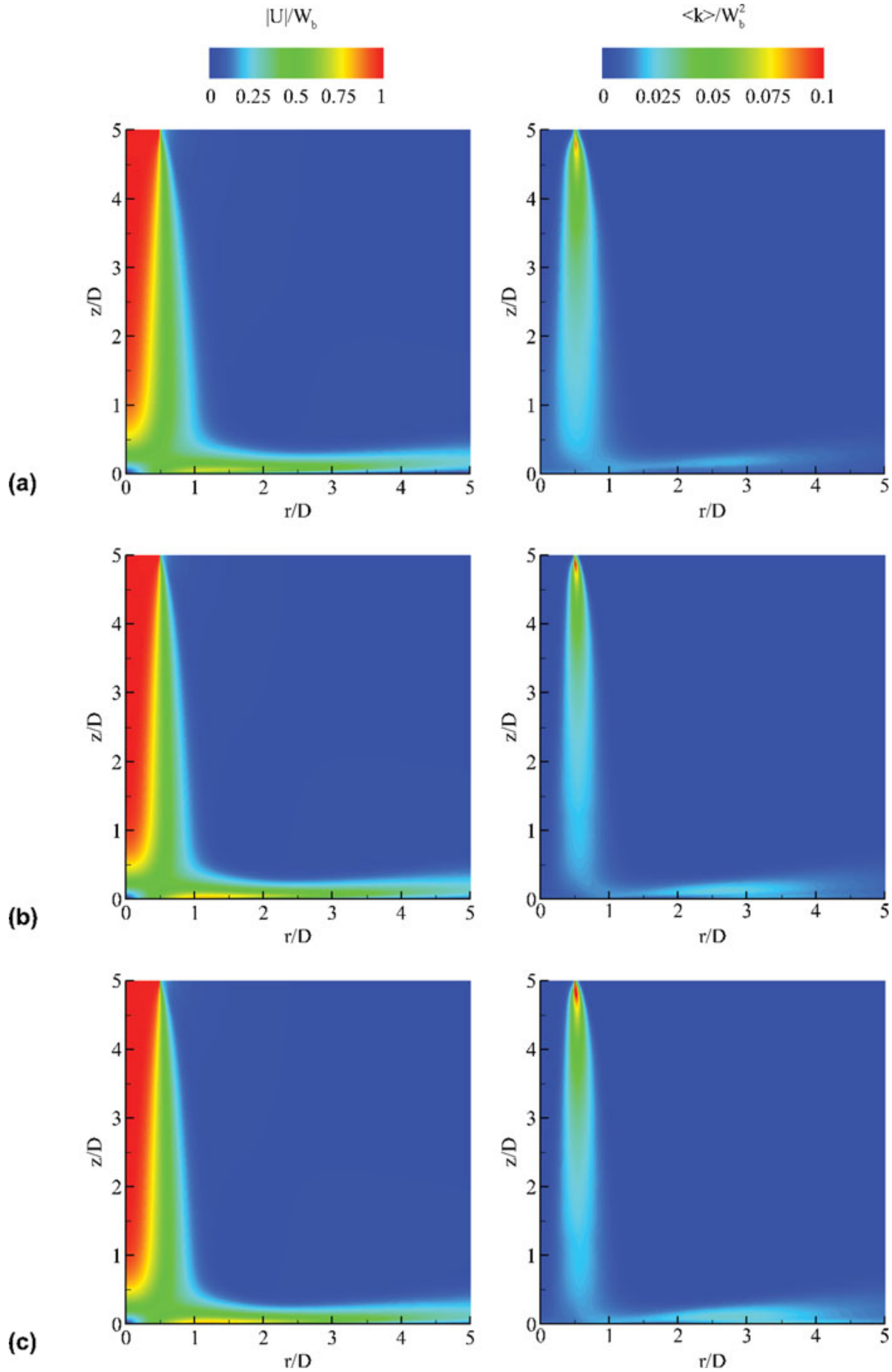

Figure 5. Comparison of maps of normalized mean velocity magnitude and turbulent kinetic energy at Reynolds numbers of (a) 4,400, (b) 10^4, and (c) 2.3×10^4, respectively.

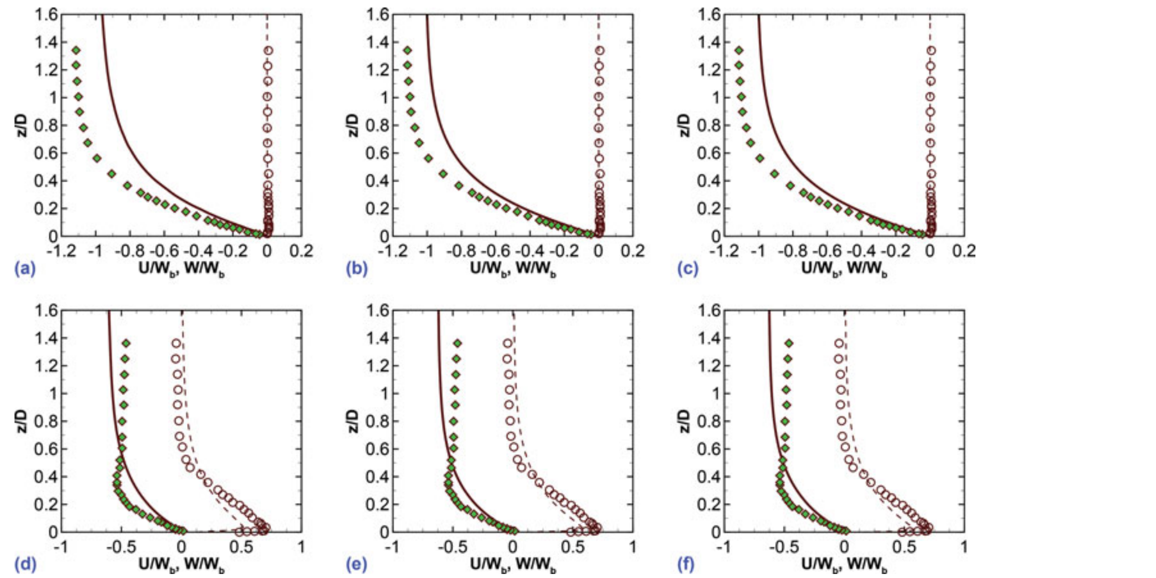

Figure 6. Comparison of velocity component in the vertical direction, (a–c) at r/D=0, Re = 4,400, 10^4, and 2.3×10^4; (d–f) at $r/D = 0.5$, Re = 4,400, 10^4, and 2.3×10^4. The data labeled by circle and diamond are obtained from Ref. [7]; solid line denotes W/Wb ; dashed line represents U/Wb.

Comparison of velocities in the vertical direction at two radial positions [$r/D = 0$, and $r/D = 0.5$] is shown in Figures 6 a–f, where experimental data labeled by open circle for U/W_b and filled diamond for W/W_b are obtained from Ref. [7]. The experimental data of Geers et al. [7] are obtained at Re = 2.3×10^4 and at a shorter orifice-to-plate distance of $H/D = 2$. At the two radial positions, predicted velocity distributions in the vertical direction agree favorably with the measured data. The discrepancy is mainly from the difference of H/D. Similarly, in the vertical direction at the two radial positions, normalized velocity distributions are insensitive to the jet Re.

However, this does not hold for distributions of velocity fluctuations, as shown in Figures 7 a–f. At the two same radial positions [$r/D = 0$, and $r/D = 0.5$], comparison of velocity fluctuations in the z-direction suggests that the jet Re does have some influence on the distribution of velocity fluctuations in the z-direction.

On the other hand, comparison of mean velocity distributions in the r-direction with the numerical results of

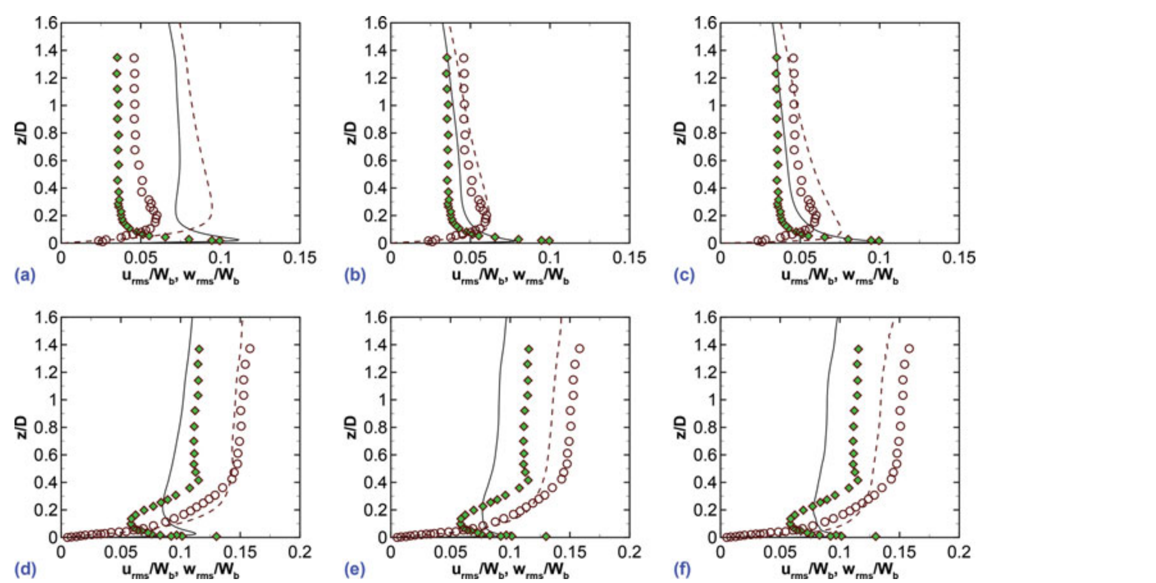

Figure 7. Comparison of velocity fluctuations in the vertical direction, (a–c) at $r/D = 0$, Re = 4,400, 10^4, and 2.3×10^4; (d–f) at $r/D = 0.5$, Re = 4,400, 10^4, and 2.3×10^4. The data labeled by circle and diamond are obtained from Ref. [7], solid line denotes u_{rms}/W_b , dashed line represents w_{rms}/W_b.

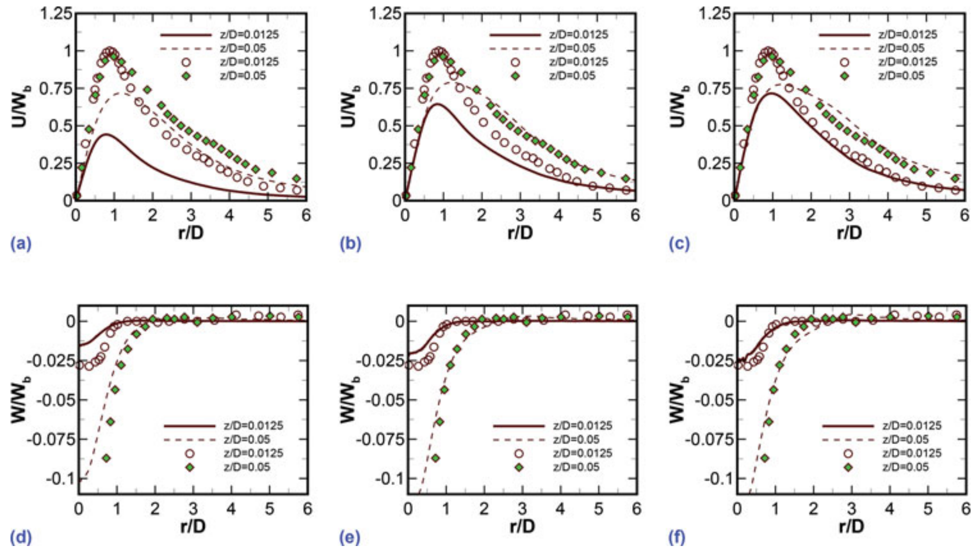

Figure 8. Comparison of mean velocity distributions in the radial direction, (a–c) for U/W_b, Re = 4,400, 10^4, and 2.3×10^4; (d–f)for W/W_b, Re = 4,400, 10^4, and 2.3×10^4. The data labeled by open circle and filled diamond are obtained from the numerical work [22].

Hadzǐabdic and Hanjalic [22] is shown in Figures 8(a)–(f), where parts (a–c) show the mean velocity component U/W_b at two distances to the wall surface ($z/D =$ 0.0125, 0.05), with (d–f) parts showing W/W_b at the two distances. In Figures 8(a)–(c), it can be seen that the radial velocity distribution is sensitive to the wall distance z/D for the three cases Re = 4,400, 10^4, 2.3×10^4. The value of mean velocity U/W_b is larger at $z/D = 0.05$ as compared with that at $z/D = 0.0125$, with the mean velocity difference depending on the distance to the impinging jet axis r/D. In Figures 8 d–f, a good agreement with numerical results as reported in Ref. [22] occurs for the wall distance $z/D = 0.05$, while for finer wall distance $z/D = 0.0125$, there is an observable discrepancy in the stagnation point region. Similarly, the discrepancy in comparison with the numerical results in Ref. [22], which are illustrated by open circles and filled diamonds, is mainly due to the difference of H/D.

The influence of round air-jet impingement condition can be seen more obviously from the comparison of turbulent stress, as shown in Figures 9 a–f. Apart from the main features such as the orifice-to-plate distance H/D and the jet Reynolds number, the assignment of boundary conditions and the numerical approach to some extent have certain influences on the LES results. From Figures 9 a–f, it is seen that at two vertical locations $z/D = 0.0125$ and 0.05, the radial distributions of sub-grid stresses indicate that there exists a clear dependence on jet Re.

Describing the target wall surface in polar coordinates, averaging the heat transfer coefficient of jet impingement in the θ-direction from zero to 2π, the heat transfer coefficient h can be expressed as a single function of r. Further averaging the local Nusselt number

$$Nu = hD/\lambda$$

in the r-direction, the mean Nusselt number can be written as

$$Nu_{av} = \frac{2}{r^2}\int_0^r Nu \cdot \eta d\eta, \tag{10}$$

where η denotes intermediate variable of integration. As shown in Figure 10, based on LES using OpenFOAM, the predicted mean Nusselt number agrees well with the data given by Ref. [4]. It can be seen that for $r/D \geq 2.5$, the data are calculated directly by empirical expression [4]

$$Nu_{av,\exp} = F \cdot [1.36\mathrm{Re}^{0.574}\mathrm{Pr}^{0.42}], \tag{11}$$

where the multiplier

$$F = [D/r(1 - 1.1D/r)]/[1 + 0.1D/r(H/D - 6)] \tag{12}$$

is a function of D/r and H/D. For the empirical Eq. (11), the available range of Reynolds number is $2,000 \leq \mathrm{Re} \leq 30,000$.

It is noted that for $r/D < 2.5$ in the region close to stagnation point, experimental data are obtained with respect to some measured curves in Ref. [4], implying that in the region there also exist some uncertainties for the empirically obtained data. In general, the favorable comparison of heat transfer indicates that the DSM-based LES with OpenFOAM can obtain satisfactory numerical heat transfer results for the normally impinging round air-jets at moderate Reynolds numbers.

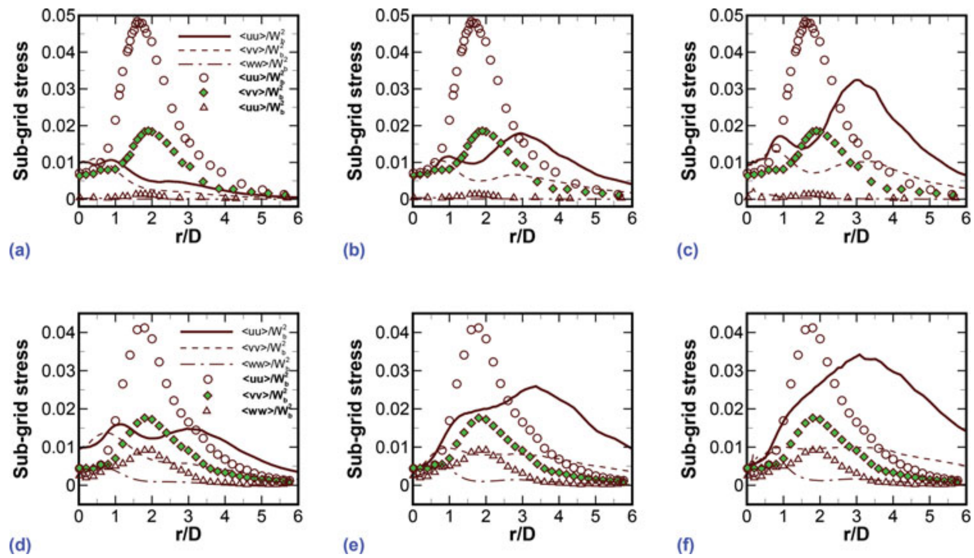

Figure 9. Comparison of turbulent stress in the radial direction (a–c) at $z/D = 0.0125$, Re = 4,400, 10^4, and 2.3×10^4; (d–f) at $z/D = 0.05$, Re = 4,400, 10^4, and 2.3×10^4. The data labeled by open circle and filled diamond are obtained from the numerical work [22].

5. Conclusions

Based on the dynamic Smagorinsky model (DSM), LES of normally impinging round air-jet heat transfer at moderate jet Reynolds numbers (4,400, 10^4, and 2.3×10^4) and at the orifice-to-plate distance $H/D = 5$ have been conducted with OpenFOAM with the following findings:

1. The normally impinging round air-jet heat transfer, and the relevant deflected turbulent flow structures on the target plate are intimately dependent on the air-jet conditions simply denoted by the jet issuing Re and the orifice-to-plate distance.
2. The mean Nusselt number based on LES agrees satisfactorily with measured empirical results, indicating that the sub-grid model DSM and OpenFOAM certainly have potential in numerically simulating some thermal engineering problems.
3. The top and side open boundaries can be assigned to have constant pressure conditions, under which reverse flow on the open boundaries is permitted.
4. To guarantee the reliability of LES results, the evaluations should be done by predicting the step ratio with the method reported recently [32].

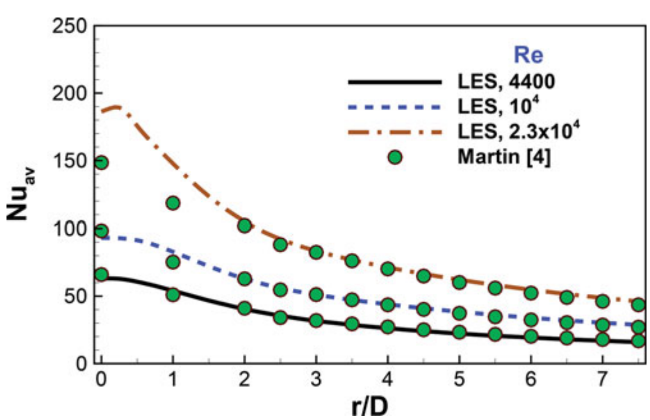

Figure 10. Distributions of mean Nusselt number at different Reynolds numbers.

Acknowledgment

This research was financially supported by National Science and Technology Ministry under Project No. 2013BAK03B08 and NSFC (51376171).

Nomenclature

c_p	specific heat capacity at constant pressure, (J/kg · K)
c_s	constant determined by the Germano identity dynamicall
D	nozzle diameter, (m
DNS	direct numerical simulation
DSM	dynamic Smagorinsky-type model
H	orifice-to-plate distance, (m)
h	heat transfer coefficient, (W/m^2 · K)
k	turbulent kinetic energy per unit mass, ($= \frac{1}{2}\overline{u'^2_i}$), (m^2/s^2)
$\langle k \rangle$	mean turbulent kinetic energy per unit mass, (m^2/s^2)
LES	large eddy simulation
Nu	Nusselt number, ($= hD/\lambda$)
Nu_{av}	mean Nusselt number
p	pressure, (Pa)
q^s_j	sub-grid heat flux, (W/m^2)
Pr	Prandtl number, ($= c_p \rho \nu / \lambda$)

Pr_s	sub-grid Prandtl number
r	radial coordinate, (m)
RANS	Reynolds averaged Navier–Stokes
Re	Reynolds number, $(= W_b D/\nu)$
R_s	ratio of maximal allowable number and actual number of time steps
S_{ij}	resolved strain rate, (s^{-1})
$S^{\max}$	assumed allowable total error
SGS	sub-grid scale
T	temperature, (K
t	time, (s)
t_0	time scale, (s)
$\bar{t}$	normalized time, $(= t/t_0)$
U	mean velocity component in radial direction, (m/s)
$\lvert U \rvert$	magnitude of velocity through the cell, (m/s)
u_τ	friction velocity, (m/s)
u_i	velocity component in x_i direction, (m/s)
u_j	velocity component in x_j direction, (m/s)
u_i'	instantaneous fluctuation of u_i, $(= \widehat{u}_i - \overline{\widehat{u}_i})$, (m/s)
u_{in}	incoming flow speed, (m/s
u_{rms}	root mean square of velocity component in radial direction, (m/s
W	mean velocity component in axial direction, (m/s)
W_b	jet-issuing mean velocity, (m/s)
w_{rms}	root mean square velocity component in axial direction, (m/s
x, y, z	Cartesian coordinates
z^+	normalized finest grid distance close to the target wall

Greek symbols

α_s	sub-grid thermal diffusivity, $(\mathrm{m}^2/\mathrm{s})$
Δ	rid filter width
δ_{ij}	Kronecker delta
λ	thermal conductivity, $(\mathrm{W/m \cdot K})$
ν	kinematic viscosity, $(\mathrm{m}^2/\mathrm{s})$
ν_s	sub-grid viscosity, $(\mathrm{m}^2/\mathrm{s})$
ρ	density, $(\mathrm{kg/m}^3)$
τ_{ij}^s	sub-grid scale stress, $(\mathrm{N/m}^2)$
$\bar{\tau}$	time period for statistical analysis in the unit of t_0

Subscripts

∞	ambient
av	average
b	bulk
exp	experimental correlations
rms	oot mean square
s	sub-grid scale
w	wall

Notes on contributors

Yongping Li is a Ph.D. student at the Department of Thermal Science & Energy Engineering, University of Science and Technology of China (USTC). He obtained his Bachelor degree of Engineering in thermal energy and power engineering from USTC in 2008. His current research interest is heat transfer caused by impinging air jets.

Liang Zhang is a Senior Engineer and a Master supervisor in the Research Institute of Chemical Defense, China. He is a member of Pyrotechnics Technical Committee of China Ordnance Society. His current research is on the heat transfer enhancement technology on ice removal using hot exhaust gas.

Qizhao Lin is a professor at USTC. He studied at the Department of Power Engineering, Dalian University of Technology and obtained his Ph.D. degree in 1988. In 2002, he undertook his work as a senior visiting scholar at the University of Texas at Austin, USA. He has been engaged in teaching and research in combustion science for 20 years.

Zuojin Zhu is an associate professor in Faculty of Engineering Science of USTC. He obtained his Ph.D. degree in 1990 at Shanghai Jiao Tong University, and worked as a research fellow at the Hong Kong Polytechnic University in 2008. His current research interest is mainly in thermal, fluid flow, and transportation engineering fields.

References

[1] Jambunathan, K., Lai, E., Moss, M. A., and Button, B. L., A Review of Heat Transfer Data for Single Circular Jet Impingement, *International Journal of Heat and Fluid Flow*, vol. 13, pp. 106–115, 1992.
[2] Viskanta, R., Heat Transfer to Impinging Isothermal Gas and Flame Jets, *Experimental Thermal Fluid Science*, vol. 6, pp. 111–134, 1993.

[3] Ichimiya, K., and Yoshida, Y., Oscillation Effect of Impingement Surface on Two-Dimensional Impingement Heat Transfer, *ASME Journal of Heat Transfer*, vol. 131, pp. 011701-1–011701-6, 2009.

[4] Martin, H., Heat and Mass Transfer Between Impinging Gas Jets and Solid Surfaces, in *Advances in Heat Transfer*, ed. P. H. James, pp. 1–60, Elsevier, New York, 1977.

[5] Baughn, J. W., and Shimizu, S., Heat Transfer Measurements From a Surface With Uniform Heat Flux and an Impinging Jet, *ASME Journal of Heat Transfer*, vol. 111, no. 4, pp. 1096–1098, 1989.

[6] Cooper, D., Jackson, D. C., Launder, B. E., and Liao, G. X., Impinging Jet Studies for Turbulence Model Assessment I. Flow-Field Experiments, *International Journal of Heat and Mass Transfer*, vol. 36, no. 10, pp. 2675–2684, 1993.

[7] Geers, L. F. G., Tummers, M. J., and Hanjalic, K., Experimental Investigation of Impinging Jet Arrays, *Experiments in Fluids*, vol. 36, pp. 946–958, 2004.

[8] Hu, G. X., and Zhang, L. X., Experimental and Numerical Study on Heat Transfer with Impinging Circular Jet on a Convex Hemispherical Surface, *Heat Transfer Engineering*, vol. 28, pp. 1008–1016, 2007.

[9] Vipat, O., Feng, S. S., Kim, T., Pradeep, A. M., and Lu, T. J., Asymmetric Entrainment Effect on the Local Surface Temperature of a Flat Plate Heated by an Obliquely Impinging Two-Dimensional Jet, *International Journal of Heat and Mass Transfer*, vol. 52, pp. 5250–5257, 2009.

[10] Yang, H. Q., Kim, T., Lu, T. J., and Ichimiya, K., Flow Structure, Wall Pressure and Heat Transfer Characteristics of Impinging Annular Jet With/Without Steady Swirling, *International Journal of Heat and Mass Transfer*, vol. 53, pp. 4092–4100, 2010.

[11] Xie, Y. H., Li, P., Lan, J. B., and Zhang, D., Flow and Heat Transfer Characteristics of Single Jet Impinging on Dimpled Surface, *ASME Journal of Heat Transfer*, vol. 135, pp. 052201(1–15), 2013.

[12] Zhang, D., Qu, H. C., Lan, J. B., Chen, J. H., and Xie, Y. H., Flow and Heat Transfer Characteristics of Single Jet Impinging on Protrusioned Surface, *International Journal of Heat and Mass Transfer*, vol. 58, pp. 18–28, 2013.

[13] Feng, S. S., Kuang, J. J., Wen, T., Lu, T. J., and Ichimiya, K., An Experimental and Numerical Study of Finned Metal Foam Heat Sinks Under Impinging Air Jet Cooling, *International Journal of Heat and Mass Transfer*, vol. 77, pp. 1063–1074, 2014.

[14] Yu, Y. Z., Zhang, J. Z., and Shan, Y., Convective Heat Transfer of a Row of Air Jets Impingement Excited by Triangular Tabs in a Confined Crossflow Channel, *International Journal of Heat and Mass Transfer*, vol. 80, pp. 126–138, 2015.

[15] Craft, T. J., Graham, L., and Launder, B. E., Impinging Jet Studies for Turbulence Model Assessment II. An Examination of the Performance of Four Turbulence Models, *International Journal of Heat and Mass Transfer*, vol. 36, no. 10, pp. 2685–2697, 1993.

[16] Park, T. S., and Sung, H. J., Development of a Near-Wall Turbulence Model and Application to Jet Impingement Heat Transfer, *International Journal of Heat and Fluid Flow*, vol. 22, no. 1, pp. 10–18, 2001.

[17] Zuckerman, N., Lior, N., Jet Impingement Heat Transfer: Physics, Correlations, and Numerical Modeling, *Advances in Heat Transfer*, vol. 39, pp. 565–631, 2006.

[18] Zhang, J. J., Xiong, Y. P., Qu, Z. G., and Tao, W. Q., Numerical Study of Flow and Heat Transfer Performance of Deflector Under Periodic Jet Impingement, *Journal of Engineering Thermophysics*, vol. 35, no. 7, pp. 1395–1400, 2014.

[19] Yalhot, V., and Orszag, S. A., Renormalization Group Analysis of Turbulence: I. Basic Theory, *Journal of Scientific Computing*, vol. 1, pp. 1–51, 1986.

[20] Olsson, M., and Fuchs, L., Large Eddy Simulations of a Forced Semiconfined Circular Impinging Jet, *Physics of Fluids*, vol. 10, no. 2, pp. 476–486, 1998.

[21] Hällqvist, T., Large Eddy Simulation of Impinging Jets with Heat Transfer, Technical Report SE-100 44, Royal Institute of Technology, Department of Mechanics, Stockholm, Sweden, 2006.

[22] Hadzǐabdic, M., and Hanjalic, K., Vortical Structures and Heat Transfer in a Round Impinging Jet, *Journal of Fluid Mechanics*, vol. 596, pp. 221–260, 2008.

[23] Uddin, N., Neumann, S. O., Weigand B., Younis, B. A., Large-Eddy Simulations and Heat-Flux Modeling in a Turbulent Impinging Jet, *Numerical Heat Transfer, Part A*, vol. 55, pp. 906–930, 2009.

[24] Nicoud, F., Toda, H. B., Cabrit, O., Bose, S., and Lee, J., Using Singular Values to Build a Subgrid-Scale Model for Large Eddy Simulations, *Physics of Fluids*, vol. 23, pp. 085106-1–085106-12, 2011.

[25] Germano, M., Piomelli, U., Moin, P., and Cabot, W., A Dynamic Subgrid-Scale Eddy Viscosity Model, *Physics of Fluids A*, vol. 3, no. 7, pp. 1760–1765, 1991.

[26] Dewan, A., Dutta, R., and Srinivasan, B., Recent Trends in Computation of Turbulent Jet Impingement Heat Transfer, *Heat Transfer Engineering*, vol. 33, no. 4–5, pp. 447–460, 2012.

[27] Toda, H. B., Cabrit, O., Truffin, K., Bruneaux, G., and Nicoud, F., Assessment of Subgrid-Scale Models with a Large-Eddy Simulation-Dedicated Experimental Database: The Pulsatile Impinging Jet in Turbulent Cross-Flow, *Physics of Fluids*, vol. 26, pp. 075108-1–07518-29, 2014.

[28] Dairay, T., Fortun, V., Lamballais, E., and Brizzi, L. E., LES of a Turbulent Jet Impinging on a Heated Wall Using High-Order Numerical Schemes, *International Journal of Heat Fluid Flow*, vol. 50, pp. 177–187, 2014.

[29] Chai, X. C., and Mahesh, K., Dynamic k-Equation Model for Large-Eddy Simulation of Compressible Flows, *Journal of Fluid Mechanics*, vol. 699, pp. 385–413, 2012.

[30] Piomelli, U., and Liu, J. H., Large-Eddy Simulation of Rotating Channel Flows Using a Localized Dynamic-Model, *Physics of Fluids*, vol. 7, no. 4, pp. 839–848, 1995.

[31] Tao, W. Q., *Numerical Heat Transfer*, pp. 333–431, Xi'an Jiantong University Press, P.R. China (in Chinese), 2001.

[32] Smirnov, N. N., Betelin, V. B., Shagaliev, R. M., Nikitin, V. F., Belyakov, I. M., Deryuguin, Yu. N., Aksenov, S. V., Korchazhkin, D. A., Hydrogen Fuel Rocket Engines Simulation Using LOGOS Code, *International Journal of Hydrogen Energy*, vol. 39, pp. 10748–10756, 2014.